FIM – Flow-Induced Motion of Three-Column Platforms

6 authors, including:

Rodolfo Trentin Gonçalves
The University of Tokyo

124 PUBLICATIONS   **831** CITATIONS

Some of the authors of this publication are also working on these related projects:

Development of a new solution of floating offshore wind turbine for Brazilian waters: Jappaku FOWT View project

Numerical Modelling of Offshore Renewables View project

FIM – Flow-Induced Motion of Three-Column Platforms

Rodolfo Trentin Gonçalves
OSPL – Ocean Space Planning Laboratory, Department of Systems Innovation, School of Engineering
University of Tokyo, Bunkyo-ku, Tokyo, Japan

Maria Eduarda Felippe Chame
TPN – Numerical Offshore Tank Laboratory, Department of Naval Architecture and Ocean Engineering
Escola Politécnica, University of São Paulo, São Paulo, SP, Brazil

Nicole Hepp Hannes
Department of Mobility Engineering, Federal University of Santa Catarina
Joinville, SC, Brazil

Pedro Paludetto Silva de Paula Lopes
TPN – Numerical Offshore Tank Laboratory, Department of Naval Architecture and Ocean Engineering
Escola Politécnica, University of São Paulo, São Paulo, SP, Brazil

Shinichiro Hirabayashi
OSPL – Ocean Space Planning Laboratory, Department of Ocean Technology, Policy, and Environment
School of Frontier Sciences, University of Tokyo, Kashiwa-shi, Chiba, Japan

Hideyuki Suzuki
OSPL – Ocean Space Planning Laboratory, Department of Systems Innovation, School of Engineering
University of Tokyo, Bunkyo-ku, Tokyo, Japan

Experiments regarding the flow-induced motion (FIM) on an array of three floating cylinders with low aspect ratio ($H/L = 15$), and three different distances between column centers ($S/L = 2$, 3, and 4) were carried out in a towing tank. The array of three cylinders was elastically supported by a set of four linear springs to provide low structural damping on the system. Three different section geometries were tested, namely, circular, square, and diamond. Three different current incident angles were tested: $\theta = 0$, 90, and 180 degrees. These configurations of the three-column arrays were selected to cover the range of the main floating offshore wind turbine (FOWT). The aims were to understand the FIM of the three-column systems and to compare the results of the single column and an array of four cylinders. The range of Reynolds numbers covered $10{,}000 < Re < 110{,}000$. Concerning the geometry of the column sections, the amplitude results showed larger amplitudes for the three-cylinder array than the single-cylinder case and the four-cylinder array for circular and diamond cases, in which cases the phenomenon was similar to vortex-induced motion (VIM). On the other hand, the amplitudes for the single square case were higher than for the array of cylinders; in this case, the galloping phenomenon was predominant. Concerning the distance between column centers, the amplitude results for the three-cylinder array with $S/L = 3$ and 4 were very similar. Yet the three-cylinder array with $S/L = 2$ acted as a single cylinder because the proximity of the cylinders changed the wakes around them. Finally, concerning the incident angle effects, the changes in the angle significantly affected the arrays with $S/L = 2$; therefore, only the in-line motions were slightly modified for the cases with the larger distances between columns.

NOMENCLATURE

A_x characteristic amplitude in the in-line direction
A_y characteristic amplitude in the transverse direction
A_{yaw} characteristic amplitude for the yaw motions
D column characteristic dimension due to the current incident angle

GM metacentric height
H column height above the water line
H_m vertical position of the mooring line fairleads
H_t height of the water level of the towing tank
H/L column aspect ratio
KG distance between the center of gravity and the base
L length of the face dimension of the column
L_m in-line position of the mooring line fairleads
L_t length of the towing tank
m mass
m^* mass ratio
R_{XX} radius of gyration around X axis
R_{YY} radius of gyration around Y axis
R_{ZZ} radius of gyration around Z axis
Re   Reynolds number

S	distance between column centers
S/L	distance between columns ratio
T_{0x}	natural period of the motion in the in-line direction in still water
T_{0y}	natural period of the motion in the transverse direction in still water
T_{0yaw}	natural period of the yaw motion in still water
U	current velocity
V_r	reduced velocity
W_m	transverse position of the mooring line fairleads
W_t	width of the towing tank
X	in-line direction
Y	transverse direction
Z	vertical direction
θ	current incident angle
$\emptyset_m$	diameter of the ring for the mooring line fairleads

INTRODUCTION

The offshore industry called attention to the vortex-induced vibrations (VIV) around single cylinders with low aspect ratio, $0.3 < H/L < 6.0$, and small mass ratio, $m^* < 6$. This specific subject was called vortex-induced motion (VIM); see Fujarra et al. (2012) for details about VIM. The studies on VIM were motivated by high current velocity incidence on circular offshore platforms, in particular cases of spar, $1.5 < H/L < 6.0$, for example, Dijk et al. (2003) and Irani and Finn (2005), and monocolumn, $0.2 < H/L < 0.5$, as in Gonçalves, Rosetti, Fujarra, Franzini, et al. (2012) and Gonçalves, Meneghini, and Fujarra (2018).

VIM has been studied on the multi-column platforms, such as semi-submersible (SS) platforms, tension leg platforms (TLP), and FOWT, as can be found in Waals et al. (2007), Gonçalves, Rosetti, Fujarra, and Oliveira (2012), Gonçalves et al. (2013), and Irani et al. (2015). Recently, the column section geometry has been considered. For example, the work by Gonçalves, Fujarra, et al. (2018) compares FIM results for circular and square column sections. Other research related to the same area includes M Liu et al. (2016) and Ramirez and Fernandes (2016), which compares VIM results for the square and diamond section columns. All these works showed that the VIM response is profoundly impacted by the column section geometry as well as by the incident angle of the current.

Moreover, Fujiwara et al. (2016) presented results concerning the effects of the distance between columns on the VIM of an SS with four columns with $S/L = 2.5$ and 4. A brief comparison between amplitudes for an array with multi-columns can be found in Gonçalves et al. (2017); in this work, a single case cylinder and an array of three and four columns were presented for 0 degrees of incidence, i.e., two side-by-side columns in the upstream position. The results of Gonçalves, Hannes, et al. (2018), for an array of four columns with different distances between columns and column geometry will be compared in the present work as well.

The development of FOWT has seen an increase because of the Japanese demand for new clean energy sources; see, for example, Wang et al. (2010) and Y Liu et al. (2016). In these works, the authors presented the new developments of FOWT and showed that the most significant number of designs are multi-column floaters with three columns. Notably, the Fukushima Floating Offshore Wind Farm Demonstration Project developed an FOWT with a three-column array in a triangular disposition, with circular and square columns, as can be seen in Fig. 1. The pioneer study on the FIM of three-column FOWT can be found in Gonçalves et al. (2019).

The study on the flow around an array of three equispaced cylinders was conducted for fixed cases, including works by Price

Fig. 1 Examples of FOWT with three columns in a triangular disposition: left, the Fukushima Mirai Wind Turbine; right, the Fukushima Shimpuu Wind Turbine
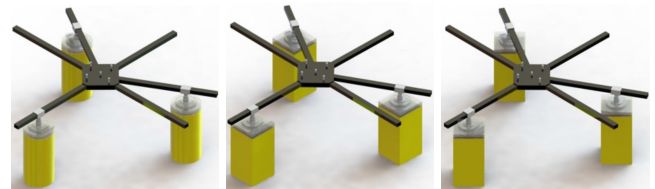

Fig. 2 Isometric view of the models with crossbar: (left) circular, (middle) square, and (right) diamond

and Paidoussis (1984), Sayers (1987), Zdravkovich (1987), Lam and Cheung (1988), and Tatsuno et al. (1998). All the works focused on showing the interference between the wakes around the array of three circular cylinders with different flow incident angles and the distance between cylinders. No research about the free cases (i.e., the array subject to the VIV) was found in the literature.

In this context, our aim here is to understand, with fundamental experiments in a towing tank, the FIM of an array of three floating cylinders with different geometric sections and the varying distance between column centers, namely $S/L = 2$, 3, and 4. The aspect ratio of the columns is $H/L = 1.5$, the typical value for these structures.

EXPERIMENTAL SETUP

All the experiments were carried out in a towing tank at the University of Tokyo, Hongo, Tokyo, Japan. The dimension of the test section is 85.0 m × 3.5 m × 2.4 m (length × width × depth). The maximum velocity of the towing car was approximately 0.4 m/s. The model was elastically supported by a set of four horizontal mooring lines; see details in Fig. 3. Figure 6 presents a schematic of the array of the three circular cylinders in the towing tank.

The circular column models were made of acrylic with external diameter $D = L = 250$ mm, as well as the square (diamond) column models with face dimension $L = 220$ mm. The cylinders did not present a roughness level and may be considered smooth cylinders. A crossbar was designed to support the three-cylinder array. The support allowed easy change of column geometry and distance between column centers, and an isometric view of the models can be seen in Fig. 1. The model's main properties can be seen in Table 1.

The six degree-of-freedom (6DOF) motions data were acquired along 70 m in the towing tank with a sampling frequency of 30 Hz using an optical motion capture system.

Nineteen different configurations were tested: circular cylinder, square, and diamond; three different distances between columns $S/L = 2$, 3, and 4; and three different angles of the current incidence as $\theta = 0$, 90, and 180 degrees. Figures 4 and 5 show the
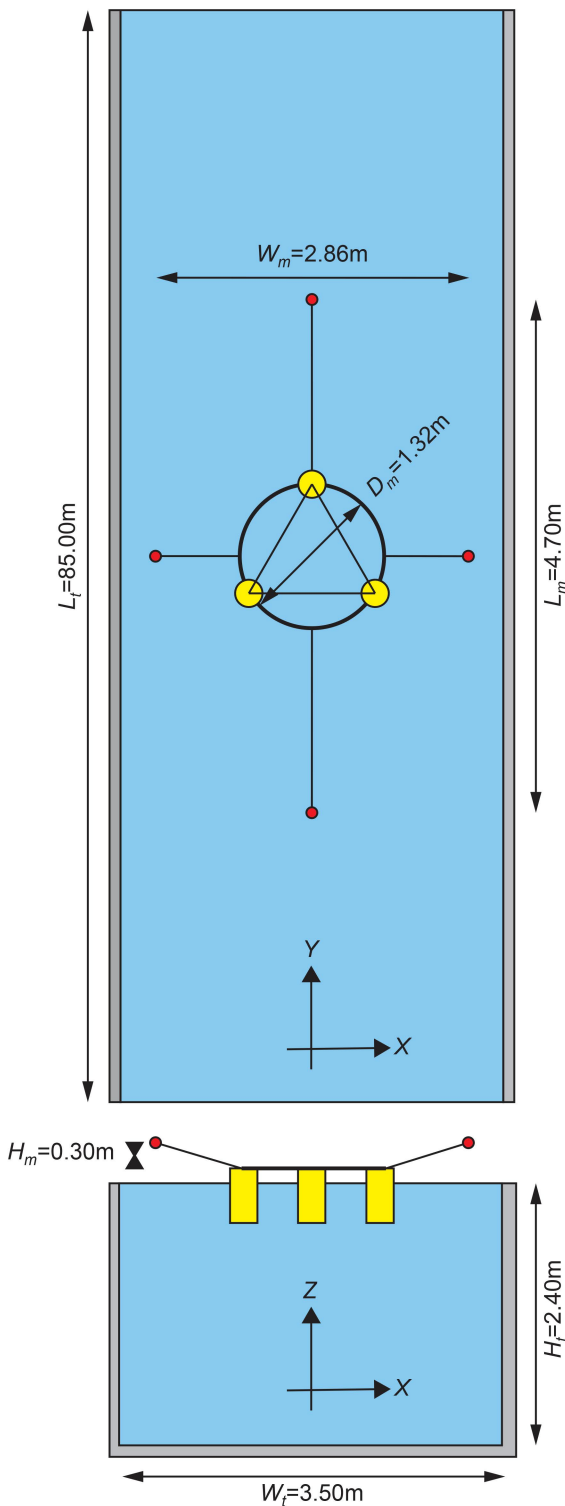
Fig. 3 Schematic of the simplified mooring system setup composed of four spring lines at the towing tank

configurations tested. The variation in the current angle of incidence was performed by changing the fairlead point in the deck above the column connections. Consequently, all the experiments were carried out with the same mooring line and stiffness configuration. Table 2 presents details about the configurations tested.

For all the cases, decay tests in still water were performed to calculate the natural frequency for the 6DOF. At least three repetitions were conducted for a better statistical result.

Property	Circular			Square/Diamond		
S/L	2	3	4	2	3	4
m [kg]	55.2	55.2	55.2	47.9	47.9	47.9
KG [mm]	194.5	194.5	194.5	190.0	190.0	190.0
GM [mm]	116.0	256.6	453.4	102.7	225.1	395.6
R_{XX} [mm]	362.0	421.0	491.7	344.4	394.8	456.0
R_{YY} [mm]	376.2	448.1	533.5	358.5	422.1	497.7
R_{ZZ} [mm]	432.0	540.4	663.7	422.6	515.2	622.1
T_{0x} [s]	13.5	13.2	12.9	13.5	13.3	13.4
T_{0y} [s]	13.6	13.3	12.8	13.8	13.6	13.6
T_{0yaw} [s]	3.7	5.6	7.2	3.3	5.0	6.4

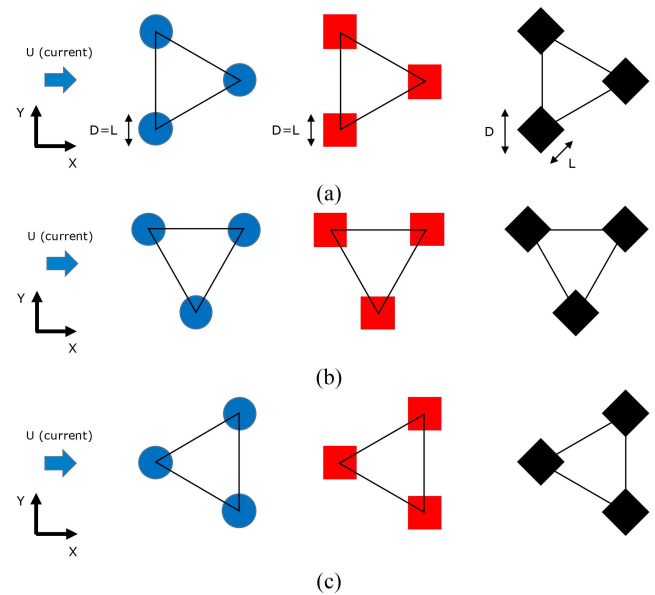Table 1 Inertia properties of the models for 0 degrees of incidence

Fig. 4 Schematic of the configurations of the three-cylinder arrays tested (circular, square, and diamond): (a) 0 degrees of incidence, (b) 90 degrees of incidence, and (c) 180 degrees of incidence
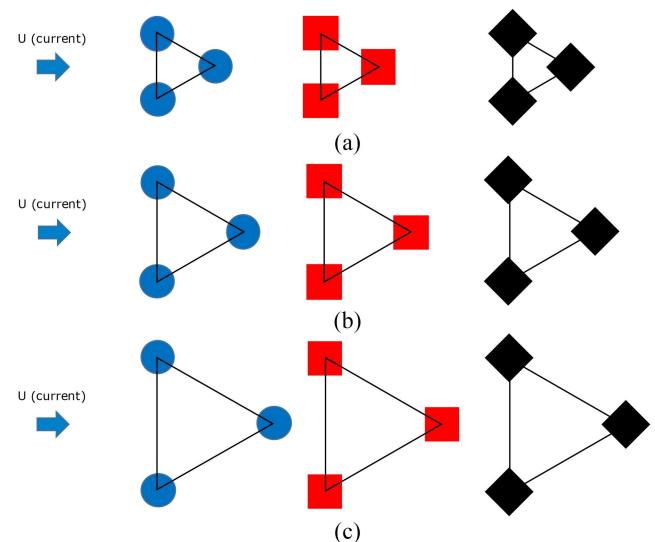

Fig. 5 Schematic of the configurations of the three-cylinder arrays tested with 0 degrees of incidence for circular, square, and diamond: (a) $S/L = 2$, (b) $S/L = 3$, and (c) $S/L = 4$
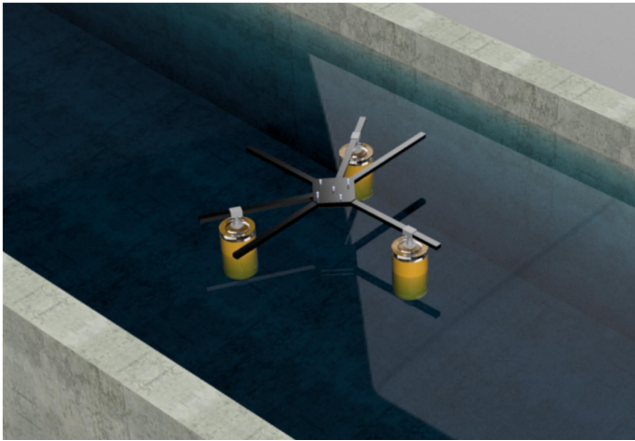
Fig. 6 Schematic of the model in the towing tank

Fig. 7 Nondimensional amplitudes for the motions in the transverse direction for the array of cylinders with $S/L = 2$

Cylinder section geometry	θ [deg]	L [mm]	D [mm]	H/L	S/L	Re $\times 10^{-3}$
Circular	0	250	250	1.5	2, 3, 4	15–65
Circular	90	250	250	1.5	3, 4	15–65
Circular	180	250	250	1.5	2, 3, 4	15–65
Square	0	220	220	1.5	2, 3, 4	10–75
Square	90	220	220	1.5	3, 4	15–100
Square	180	220	220	1.5	3, 4	10–75
Diamond	0	220	311	1.5	2, 3	25–110
Diamond	90	220	311	1.5	—	—
Diamond	180	220	311	1.5	2, 4	25–110

Table 2   Matrix of conditions carried out for FIM studies of the three-cylinder arrays

METHODOLOGY

The FIM response was analyzed through the root mean square (RMS) of displacements in the transverse and in-line directions and angles of rotation in the case of the yaw motion. The nominal amplitudes were calculated as $\sqrt{2}$ times the RMS displacements. Moreover, as commonly found, dimensionless values A_x/L and A_y/L were presented using the face dimension of the column, L. For the RMS angles of yaw, A_{yaw}, no dimensionless presentation was adopted, as is usual in the literature.

The reduced velocity $V_r = UT_{0y}/D$ was defined as a function of the incident current velocity U, the natural period of the transverse motion in still water T_{0y}, and the characteristic length of the body section subjected to vortex shedding D. In this case, D can be written as a function of the current incident angle for square columns, to better represent the characteristic length of the column section on the flow; i.e., $D = L(|\sin\theta| + |\cos\theta|)$, where θ is the current incident angle. For circular column cases, $D = L$ for all incident angles.

RESULTS

Figures 7–9 present the characteristic amplitudes for the array of cylinders with $S/L = 2$, $\theta = 0$ and 180 degrees, and different column geometries.

The results showed a significant difference due to the column section geometry for $S/L = 2$. The amplitudes were the largest for circular column cases for all the main degrees of freedom, namely, in-line, transverse, and yaw.
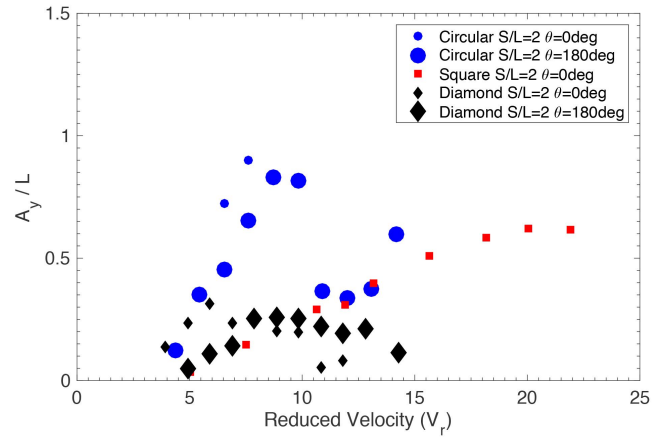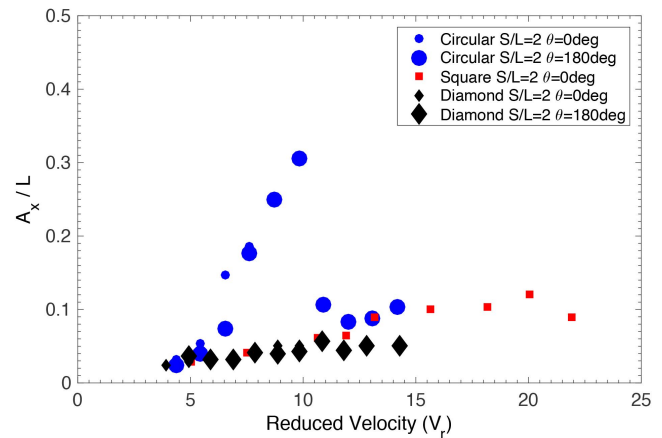

Fig. 8 Nondimensional amplitudes for the motions in the in-line direction for the array of cylinders with $S/L = 2$
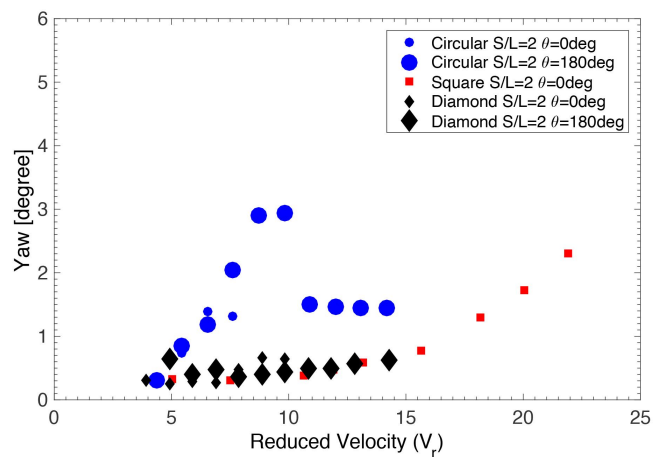

Fig. 9 Yaw motion amplitudes for the array of cylinders with $S/L = 2$

The incident angles, $\theta = 0$ and 180 degrees, did not affect the amplitude significantly in the in-line direction or yaw motion results for $S/L = 2$. Some differences can be observed only for the amplitudes in the transverse direction (see Fig. 7); the amplitudes were higher for $\theta = 0$, i.e., in the conditions in which the two side-

by-side columns are in the upstream position. The explanation for this is that the wake interference was acting only on the unique column downstream and decreased the total lift force of the system; in the other case, in which one column was in the upstream position, the wake interfered with the two columns downstream and caused a more significant decrease in the lift force.

The amplitudes in the transverse direction (see Fig. 7) showed different behaviors for the circular/diamond cases compared with the square case. The amplitudes for the circular/diamond cases presented a local maximum; i.e., it was possible to observe an increase and decrease of amplitudes around $V_r = 8$, and this behavior is similar to the resonance range in the VIM phenomenon. In turn, an increase can be observed in the amplitudes when increasing the reduced velocity for the square column cases; this behavior is similar to the galloping phenomenon. Because of this finding, it is better, for now, to call the general behavior of multi-columns subject to the current incidence FIM and no longer only VIM as is typically encountered in the literature. It is important to say that the FIM is specific for each system geometry, and any modification (such as the inclusion of pontoons, for example) can change the flow around the system entirely and, consequently, the response. In Fig. 8, the maximum values of the amplitudes in the transverse direction for $S/L = 2$ were $A_y/L = 0.9$, 0.6, and 0.3 for the circular, square, and diamond cases, respectively.

The amplitudes in the in-line direction and yaw motions are presented in Figs. 8 and 9, respectively. The amplitudes in the in-line direction (see Fig. 8) showed a significant difference for the circular cases, in which it is possible to observe the resonance phenomenon (presence of the amplitude drop) and maximum amplitude $A_x/L = 0.3$. For the square/diamond cases, the behavior of the amplitudes in the in-line direction was almost the same up to $V_r = 11$; after this velocity, the amplitudes for the square case kept growing, which again confirmed the galloping behavior for the square cases. The maximum amplitudes for the square/diamond cases were lower than for the circular cases ($A_x/L = 0.15$ and 0.05 for the square and diamond cases, respectively). No difference due to the incident angle was observed for this degree of freedom.

As in the results of amplitudes in the in-line direction, in the results of amplitudes of the yaw motion (see Fig. 9) the behavior was the same as discussed before. The maximum values of the amplitudes of the yaw motion for $S/L = 2$ were $A_{yaw} = 3.0$, 2.5, and 1.0 degrees for the circular, square, and diamond cases, respectively. The galloping behavior was pronounced for the square case, in which high reduced velocities could be reached, $V_r < 23$.

Figure 10 presents the nondimensional frequency for the array of cylinders with $S/L = 2$, $\theta = 0$ and 180 degrees, and different column geometries. The results showed that the motions in the transverse direction were concentrated around the natural frequency in still water for this degree of freedom. This behavior is quite similar to the galloping behavior characteristic. For the VIM phenomenon, synchronization between the vortex shedding and the motion of the system occurs; therefore, an increase of the nondimensional frequency is observed with an increase of the reduced velocity. This behavior could be found for the diamond cases for $V_r < 13$. A conclusion could not be drawn about the FIM source because of the small number of reduced velocities tested.

Figures 11–13 present the characteristic amplitudes for the array of cylinders with $S/L = 3$; $\theta = 0$, 90, and 180 degrees; and different column geometries.

The results showed considerable difference because of the column section geometry for $S/L = 3$. The amplitudes were the largest for circular column cases for all the degrees of freedom,
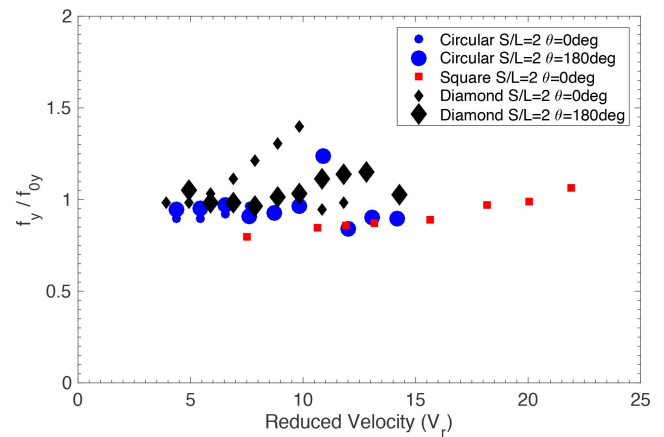
Fig. 10 Nondimensional frequency for the motions in the transverse direction for the array of cylinders with $S/L = 2$

namely, in-line, transverse, and yaw. Only for the amplitudes in the transverse direction were the results for circular and diamond cases comparable.

The incident angles, $\theta = 0$, 90, and 180 degrees, did not affect the amplitude significantly in the transverse direction for $S/L = 3$. Some differences can be observed only for the circular columns case in the in-line direction and yaw motions.
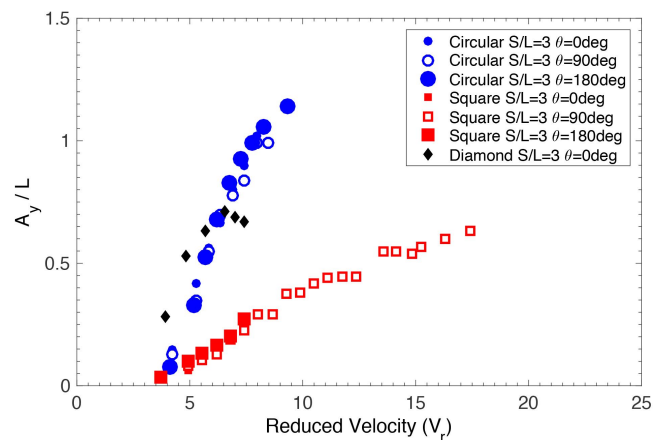
Fig. 11 Nondimensional amplitudes for the motions in the transverse direction for the array of cylinders with $S/L = 3$
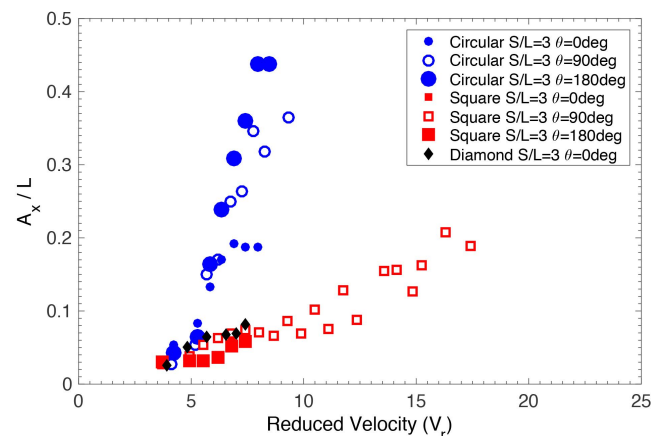
Fig. 12 Nondimensional amplitudes for the motions in the in-line direction for the array of cylinders with $S/L = 3$

The amplitudes in the transverse direction (see Fig. 11) showed different behaviors for the circular, square, and diamond cases. The amplitudes presented a local maximum only for the diamond column case, around $V_r = 6$; this behavior can confirm the VIM phenomenon. On the other hand, it is not possible to observe a decrease in amplitudes when increasing the reduced velocities for the circular and square column cases. The galloping behavior can be confirmed for the square case because high values of reduced velocities were used. However, it cannot be established for the circular column cases due to the limitation in the reduced velocity tested, $V_r < 10$.

In Fig. 11, the maximum values of the amplitudes in the transverse direction for $S/L = 3$ were $A_y/L = 1.25$, 0.70, and 0.75 for the circular, square and diamond cases, respectively. No difference due to the incident angle was observed for this degree of freedom.

For the in-line direction (see Fig. 12), the amplitude results showed an increase in the amplitudes with the increase in the reduced velocity for all the column geometries; the galloping behavior can explain these results in the in-line direction. The amplitude results for $\theta = 180$ degrees were the highest and the ones for $\theta = 0$ degrees were the lowest; moreover, the results for $\theta = 90$ degrees presented similar behavior to those for $\theta = 180$ degrees, but the amplitudes were smaller. The position of the columns downstream affected mainly the drag forces.

The maximum values of the amplitudes in the in-line direction for $S/L = 3$ were $A_x/L = 0.45$, 0.2, and 0.1 for the circular, square, and diamond cases, respectively.

For the yaw motions (see Fig. 13), the amplitude results showed the same behavior as that presented for the in-line direction; the galloping behavior can thus be confirmed for the range of reduced velocities tested. The yaw motion was very low for the diamond column case. The incident angle affected the results. The explanation for the yaw motion is that the coherence between wakes decreased because of the geometric asymmetry to the flow incidence for $\theta = 90$ degrees; consequently, so did the yaw moment in the system. The substantial result variations for the cases with $\theta = 90$ were due to the nonsymmetric flow incidence (two columns on one side and one column on the other), mainly for the circular case in which the points for the separation of the vortex shedding were not well defined.

The maximum values of the amplitudes of the yaw motions for $S/L = 3$ were $A_{yaw} = 5.0$, 4.0, and 0.5 degrees for the circular, square, and diamond cases, respectively.

Figure 14 presents the nondimensional frequency for the array of cylinders with $S/L = 3$; $\theta = 0$, 90, and 180 degrees; and dif-
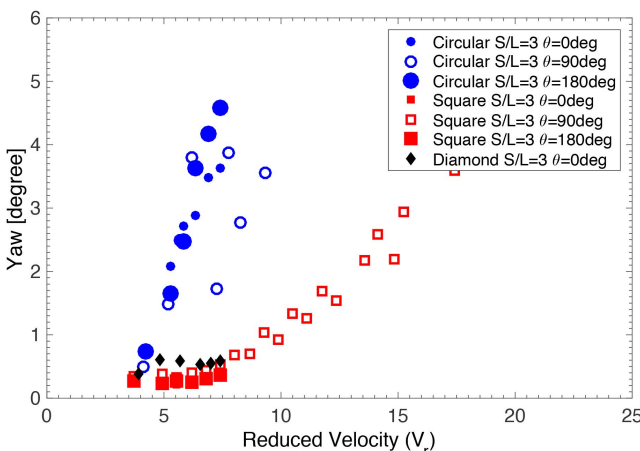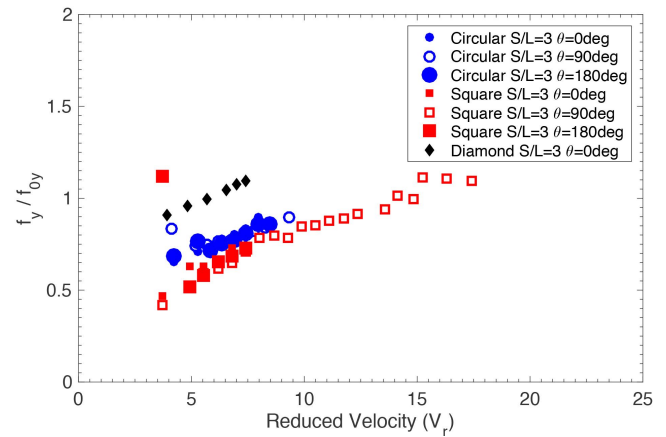

Fig. 14 Nondimensional frequency for the motions in the transverse direction for the array of cylinders with $S/L = 3$

ferent column geometries. For all the cases, an increase in the nondimensional frequency with increasing reduced velocity was observed mainly for $V_r < 15$. This behavior is a typical VIM phenomenon characteristic. These results complement the discussion of the amplitudes in the transverse direction presented before.

Figures 15–17 present the characteristic amplitudes for the array of cylinders with $S/L = 4$; $\theta = 0$, 90, and 180 degrees; and
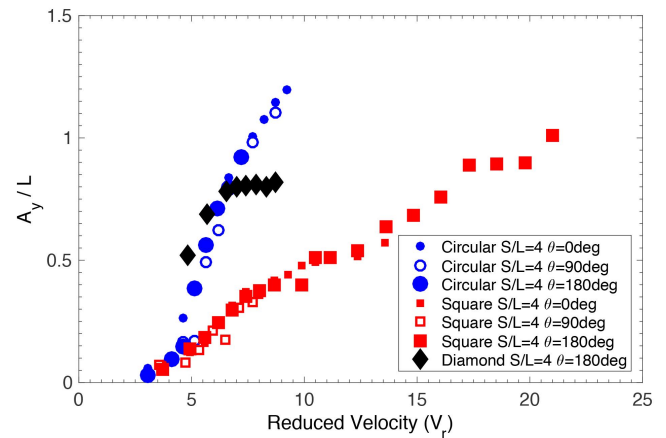

Fig. 15 Nondimensional amplitudes for the motions in the transverse direction for the array of cylinders with $S/L = 4$

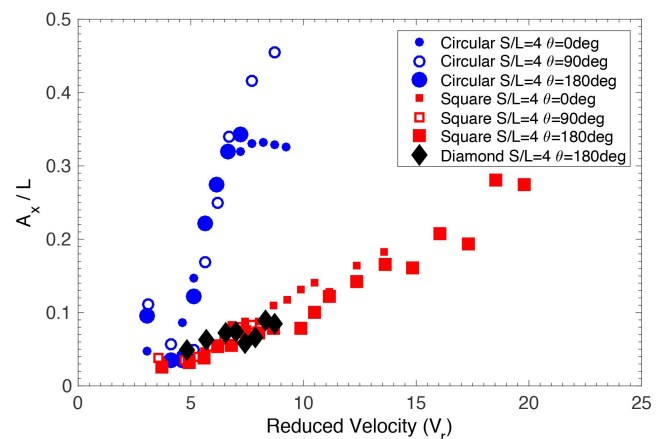Fig. 13 Yaw motion amplitudes for the array of cylinders with $S/L = 3$

Fig. 16 Nondimensional amplitudes for the motions in the in-line direction for the array of cylinders with $S/L = 4$

different column geometries. The amplitude results in the transverse direction (see Fig. 15) showed no difference due to the current incident angle for all the column geometries. The results differed for each geometry, and the galloping behavior with an increase in the amplitude gained by increasing the reduced velocity can be observed for the circular and square cases for the velocities tested for each geometry. For the diamond case, a constant amplitude can be verified after $V_r > 7$. The maximum values of the amplitudes in the transverse direction for $S/L = 4$ were $A_y/L = 1.3$, 1.0, and 0.8 for the circular, square, and diamond cases, respectively.

In the amplitude results in the in-line direction (see Fig. 16), it was possible to see the current incident angle effects only for the circular case when comparing $\theta = 0$ and 180 degrees, because of the significant impact on the drag forces, mainly the fluctuation part. The in-line amplitudes presented the same behavior for the square and diamond column cases. The maximum values of the amplitudes in the in-line direction for $S/L = 4$ were $A_x/L = 0.5$, 0.3, and 0.1 for the circular, square, and diamond cases, respectively.

The results of the amplitudes of yaw motion (see Fig. 17) were dispersed in the region of $3 < V_r < 7$ mainly for the circular column case. For both geometries, the yaw motion increased with the increase of reduced velocity. The galloping behavior was confirmed for this degree of freedom. The maximum values of the amplitudes of the yaw motions for $S/L = 4$ were $A_{yaw} = 5.0$, 4.0, and 2.0 degrees for the circular, square, and diamond cases, respectively.

Figure 18 presents the nondimensional frequency for the array of cylinders with $S/L = 3$; $\theta = 0$, 90, and 180 degrees; and different column geometries. Only the square case presented a constant nondimensional frequency around the natural frequency for $V_r > 7$. This result can confirm the galloping characteristic of the square case for high values of reduced velocity. For the other cases, circular and diamond, the VIM behavior was observed. The same results and conclusions were drawn by Zhao et al. (2014) for square cylinders with high aspect ratio; i.e., cylinders with square sections and 0 degrees of incidence presented mainly galloping behavior, and ones with 45 degrees of incidence presented mostly VIM phenomenon.

In Fig. 19, the amplitude results in the transverse direction were consolidated to clarify the distance between column center effects, $S/L = 2$, 3, and 4. The results were presented for all the column geometry cases for $\theta = 0$ or 180 degrees. As noted before, the
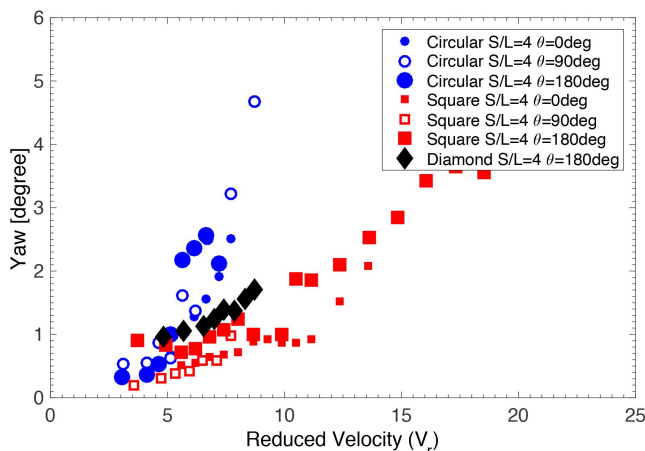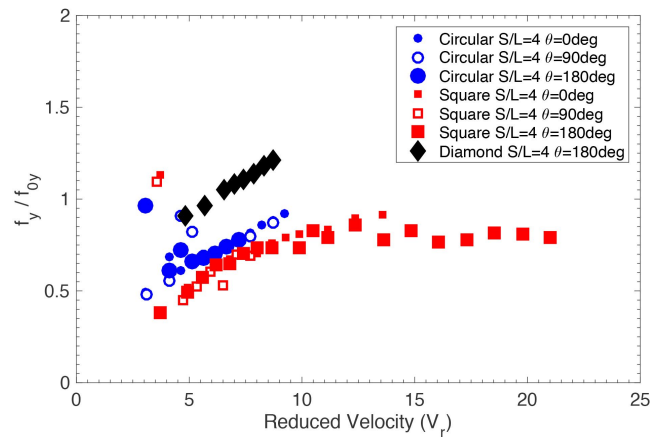

Fig. 18 Nondimensional frequency for the motions in the transverse direction for the array of cylinders with $S/L = 4$

amplitude in the transverse direction did not differ in these incident angles.

The amplitudes in the transverse direction were practically the same for all the values of the distance between columns for the circular case. Thus, the distance between columns did not affect this column geometry. On the other hand, the amplitude results were very different when comparing the cases of $S/L = 2$ and the large distances for the square and diamond cases. In the diamond and square cases, the amplitudes were lower when the distance between the column centers was smaller; i.e., the amplitudes in the transverse direction decreased when the distance between column ratios decreased.

For the diamond and square cases with $S/L = 2$, the distance between the columns was so small that the flow around the array of three columns could be considered the flow around a single column (see details of the geometry in Fig. 5a); i.e., the characteristic diameter D of the system can be considered the whole system. This consideration can explain the shift to the right in the amplitude curve for the square case, and the maximum amplitude in $V_r = 5$ for the diamond case.

Figure 20 shows the consolidated comparison between the results for the single-cylinder case and the arrays of three and four cylinders for 0 degrees of incidence. All the column geometries were considered. The results of a single-cylinder and a four-cylinder array were reported in Gonçalves et al. (2017) and are presented here again for comparison.

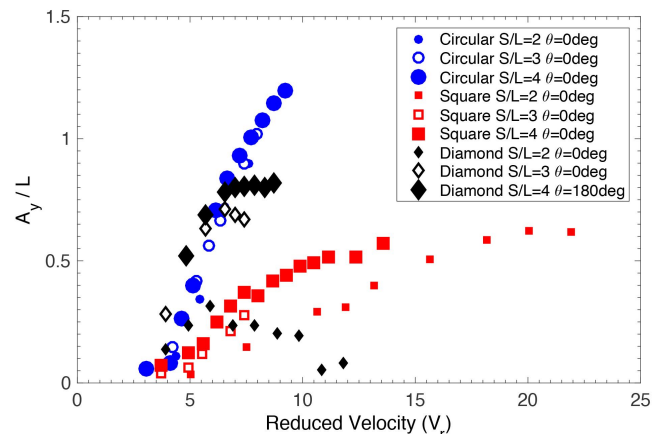Fig. 17 Yaw motion amplitudes for the array of cylinders with $S/L = 4$

Fig. 19 Nondimensional amplitudes for the motions in the transverse direction for the array of cylinders for $\theta = 0$ degrees
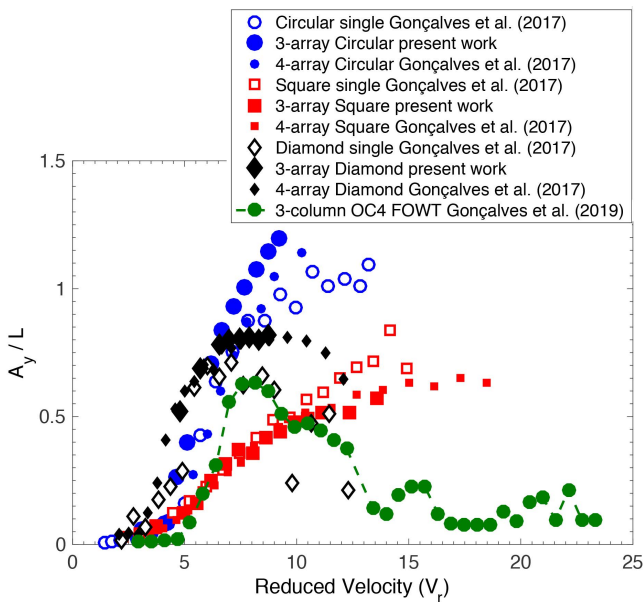
Fig. 20 Comparison of the nondimensional amplitudes for the motions in the transverse direction for the single-cylinder case and the array of cylinders with three and four columns

For the circular and diamond cases, the three-cylinder array presented the highest amplitudes in the transverse direction, and the single circular cylinder presented the lowest amplitudes. Because the behavior of the transverse amplitudes for circular and diamond cases is practically the same, it is possible to conclude that the FIM, in this case, can be considered VIM; i.e., the motions are due to the vortex shedding around the cylinders, and a resonance region is expected as in the diamond case. The resonance behavior could not be confirmed by the circular case because of the low reduced velocity range tested.

For the square case, the single cylinder presented the highest amplitudes in the transverse direction, and the results for the array of cylinders were almost the same independent of the number of cylinders (three or four). The behavior differed for the square case because the predominant FIM, in this case, was galloping.

The comparison with the results for the three-column OC4 platform showed lower amplitudes for the last case because of the presence of an additional center column and also connectors between the columns. These geometries interfered in the wake around the system and affected the amplitudes. Thus, the effects of pontoons, connectors, and additional columns need to be better studied to help the designers.

As observed in all the results, higher reduced velocities were reached for the square case. The limit of the reduced velocity performed was due to the limitation of the drift of the model. In the cases in which FIM (resonance behavior for circular and diamond cases) occurred, amplification of the drag phenomenon was observed; therefore, the model drift was larger than the limit of monitoring. On the other hand, in the cases in which galloping occurred, the drift was smaller, thus justifying the higher reduced velocity points.

CONCLUSIONS

Experimental studies were conducted in a towing tank to evaluate the FIM behavior of the three-cylinder array. In order to understand the effects of the different parameters on the FIM, three different ones were used in the experiments, such as column

geometry (circular, square, and diamond), the distance between column centers ($S/L = 2$, 3, and 4), and current incident angles ($\theta = 0$, 90, and 180 degrees).

The column geometry markedly affects the FIM behavior of the three-cylinder array. The most considerable amplitudes were observed for the circular case for the motions in the transverse and in-line directions and yaw. For the transverse direction, VIM behavior was confirmed for the circular and diamond cases; however, galloping behavior was confirmed for the square case. For yaw motions, all the geometries presented similarities in the galloping behavior. Tests for measuring the forces for different incident angles of the current must be performed to conclude that the source of the FIM is galloping or VIM. In this work, some evidence about the origin of the FIM was presented, but the evidence still needs to be completed with additional model tests.

The distance between column centers showed a different behavior for $S/L = 2$, in which the columns acted as a single body to the flow incidence. This behavior was observed for the diamond and square cases. For $S/L = 3$ and 4, the results were practically the same, which allows the conclusion that, for $S/L > 3$, the effect of the distance between column centers can be neglected.

The current incident angles affected mainly the in-line motion when the drag force was modified by the columns downstream. The difference between the results for $\theta = 0$ and 180 degrees can be neglected. The yaw motion results for $\theta = 90$ degrees differed from other incident angles due to the asymmetry of the system, but the maximum amplitudes were quite similar.

Finally, the comparison of the present work with previous work in the literature about the VIM of a system with a different number of cylinders for 0 degrees of incidence showed higher amplitudes in the transverse direction occurring for the three-cylinder array than for the single-cylinder and four-cylinder array, for the circular and diamond cases; moreover, the highest amplitude occurred for the single square case when compared with the arrays of square cylinders.

All of these conclusions show the importance of better understanding the FIM of the array of cylinders and how the parameters can influence the motion amplitudes. The results presented here are essential for designing floating offshore platforms and FOWT, and can also provide benchmark data for computational fluid dynamics (CFD).

Further studies will present the same results shown here for a four-cylinder array, adding the comparison for a system with and without the presence of pontoons.

REFERENCES

Dijk, RR, Magee, A, Perryman, S, and Gebara, J (2003). "Model Test Experience on Vortex-Induced Vibrations of Truss Spars," *Proc Offshore Technol Conf*, Houston, TX, USA, OTC2003-15242. https://doi.org/10.4043/15242-MS.

Fujarra, ALC, Rosetti, GF, Wilde, J, and Gonçalves, RT (2012). "State-of-Art on Vortex-Induced Motion: A Comprehensive Survey After More Than One Decade of Experimental Investigation," *Proc ASME 31st Int Conf Ocean Offshore Arct Eng*, Rio de Janeiro, Brazil, 4, 561–582. https://doi.org/10.1115/OMAE2012-83561.

Fujiwara, T, Nimura, T, Shimozato, K, and Matsui, R (2016). "VIM Model Test and Assessment on a Semi-Submersible Type Floater with Different Column Intervals," *Proc ASME 35th Int Conf Ocean Offshore Arct Eng*, Busan, Korea, 1, V001T01A055. https://doi.org/10.1115/OMAE2016-54308.

Gonçalves, RT, Chame, MEF, Hannes, NH, et al. (2017). "Experimental Flow-Induced Motions of Array of Floating Cylinders with Circular, Square and Diamond Sections," *Proc 24th ABCM Int Congr Mech Eng*, Curitiba, Brazil, COBEM-2017-0441. https://doi.org/10.26678/ABCM.COBEM2017.COB17-0441.

Gonçalves, RT, Chame, MEF, Silva, LSP, et al. (2019). "Experimental Study on Flow-Induced Motions (FIM) of a Floating Offshore Wind Turbine Semi-Submersible Type (OC4 Phase II Floater)," *Proc ASME 2nd Int Offshore Wind Tech Conf*, St Julian's, Malta, V001T01A017. https://doi.org/10.1115/IOWTC2019-7513.

Gonçalves, RT, Fujarra, ALC, Rosetti, GF, Kogishi, AM, and Koop, A (2018). "Experimental Study of the Column Shape and the Roughness Effects on the Vortex-Induced Motions of Deep-Draft Semi-Submersible Platforms," *Ocean Eng*, 149, 127–141. https://doi.org/10.1016/j.oceaneng.2017.12.013.

Gonçalves, RT, Hannes, NH, et al. (2018). "Experimental Study on Flow-Induced Motion of an Array of Four Cylinders with Different Spacing Ratio," *Proc OCEANS 18 MTS/IEEE Kobe/Techno-Ocean 2018*, Kobe, Japan. https://doi.org/10.1109/OCEANSKOBE.2018.8559253.

Gonçalves, RT, Meneghini, JR, and Fujarra, ALC (2018). "Vortex-Induced Vibration of Floating Circular Cylinders with Very Low Aspect Ratio," *Ocean Eng*, 154, 234–251. https:// doi.org/10.1016/j.oceaneng.2018.02.019.

Gonçalves, RT, Rosetti, GF, Fujarra, ALC, Franzini, GR, et al. (2012). "Experimental Comparison of Two Degrees-of-Freedom Vortex-Induced Vibration on High and Low Aspect Ratio Cylinders with Small Mass Ratio," *J Vib Acoust*, 134(6), 061009. https://doi.org/10.1115/1.4006755.

Gonçalves, RT, Rosetti, GF, Fujarra, ALC, and Oliveira, AC (2012). "Experimental Study on Vortex-Induced Motions of a Semi-Submersible Platform with Four Columns, Part I: Effects of Current Incidence Angle and Hull Appendages," *Ocean Eng*, 54, 150–169. https://doi.org/10.1016/j.oceaneng.2012.06.032.

Gonçalves, RT, Rosetti, GF, Fujarra, ALC, and Oliveira, AC (2013). "Experimental Study on Vortex-Induced Motions of a Semi-Submersible Platform with Four Columns, Part II: Effects of Surface Waves, External Damping and Draft Condition,"

Ocean Eng, 62, 10–24. https://doi.org/10.1016/j.oceaneng.2013.01.019.

Irani, M, and Finn, L (2005). "Improved Strake Design for Vortex-Induced Motions of Spar Platforms," *Proc ASME 24th Int Conf Offshore Mech Arct Eng*, Halkidiki, Greece, 1, 767–773. https://doi.org/10.1115/OMAE2005-67384.

Irani, M, Jennings, T, Geyer, J, and Krueger, E (2015). "Some Aspects of Vortex-Induced Motions of a Multi-Column Floater," *Proc ASME 34th Int Conf Ocean Offshore Arct Eng*, St John's, Canada, 2, V002T08A036. https://doi.org/10.1115/OMAE2015-41164.

Lam, K, and Cheung, C (1988). "Phenomena of Vortex Shedding and Flow Interference of Three Cylinders in Different Equilateral Arrangements," *J Fluid Mech*, 196, 1–26. https://doi.org/10.1017/S0022112088002587.

Liu, M, Xiao, L, Lu, H, and Shi, J (2016). "Experimental Investigation into the Influences of Pontoon and Column Configuration on Vortex-Induced Motions of Deep-Draft Semi-Submersibles," *Ocean Eng*, 123, 262–277. https://doi.org/10.1016/j.oceaneng.2016.07.007.

Liu, Y, Li, S, Yi, Q, and Chen, D (2016). "Developments in Semi-Submersible Floating Foundations Supporting Wind Turbines: A Comprehensive Review," *Renewable Sustainable Energy Rev*, 60, 433–449. https://doi.org/10.1016/j.rser.2016.01.109.

Price, SJ, and Paidoussis, MP (1984). "The Aerodynamic Forces Acting on Groups of Two and Three Circular Cylinders When Subject to a Cross-Flow," *J Wind Eng Ind Aerodyn*, 17(3), 329–347. https://doi.org/10.1016/0167-6105(84)90024-2.

Ramirez, MAM, and Fernandes, AC (2016). "Novel Experimental Investigation on Vortex-Induced Motions of a Tension Leg Platform," *Proc ASME 35th Int Conf Ocean Offshore Arct Eng*, Busan, Korea, 2, V002T08A058. https://doi.org/10.1115/OMAE2016-54530.

Sayers, AT (1987). "Flow Interference Between Three Equispaced Cylinders with Subjected to a Cross Flow," *J Wind Eng Ind Aerodyn*, 26(1), 1–19. https://doi.org/10.1016/0167-6105(87)90033-X.

Tatsuno, M, Amamoto, H, and Ishi-I, K (1998). "Effects of Interference Among Three Equidistantly Arranged Cylinders in a Uniform Flow," *Fluid Dyn Res*, 22(5), 297–315. https://doi.org/10.1016/S0169-5983(97)00040-3.

Waals, OJ, Phadke, AC, and Bultema, S (2007). "Flow-Induced Motions of Multi-Column Floaters," *Proc ASME 26th Int Conf Offshore Mech Arct Eng*, San Diego, CA, USA, 1, 669–678. https://doi.org/10.1115/OMAE2007-29539.

Wang, CM, Utsunomiya, T, Wee, SC, and Choo, YS (2010). "Research on Floating Wind Turbines: A Literature Survey," *IES J Part A: Civil Struct Eng*, 3(4), 267–277. https://doi.org/10.1080/19373260.2010.517395.

Zdravkovich, MM (1987). "The Effects of Interference Between Circular Cylinders in Cross Flow," *J Fluids Struct*, 1(2), 239–261. https://doi.org/10.1016/S0889-9746(87)90355-0.

Zhao, J, Leontini, JS, Jacono, DL, and Sheridan, J (2014). "Fluid–Structure Interaction of a Square Cylinder at Different Angles of Attack," *J Fluid Mech*, 747, 688–721. https://doi.org/10.1017/jfm.2014.167.